

Nonlinear stability of the near-Earth plasma sheet during substorms: 9 February 1995 event

P. Dobias, J.A. Wanliss, and J.C. Samson

Abstract: It has been previously demonstrated that several minutes prior to an onset of a magnetospheric substorm the near-Earth plasma sheet becomes unstable to resonance-type perturbations. The next logical step, examined here, is an assumption that the velocity shear in the resonance would lead to a development of a Kelvin–Helmholtz (KH) instability. Using a Grad-Shafranov equilibrium constrained by CANOPUS data, we analyze the stability properties of the near-Earth plasma sheet in the presence of a field-line resonance-generated KH instability at around 10 Earth radii. The results of the analysis are in general agreement with observations and computer modeling of substorms. As a part of the analysis, we discuss the importance of the proper distinction between the stability properties of the magnetotail, and the trigger mechanism responsible for the instability. While these two aspects of a substorm may be (and likely are) related, it is possible that they involve different types of processes that work in a complementary fashion.

PACS Nos.: 06.54, 27.40, 27.72, 27.88

Résumé : Il a déjà été montré que plusieurs minutes avant le début d'une sous-tempête magnétique, la couche de plasma voisine de la Terre devient sensible aux perturbations de type résonant. La prochaine étape logique qui est étudiée ici, est de supposer que la vitesse de déchirement dans la résonance mènerait au développement d'une instabilité de Kelvin–Helmholtz (K–H). Utilisant un équilibre à la Grad-Shafranov rendu cohérent avec les données de CANOPUS, nous analysons les propriétés de stabilité de la couche de plasma voisine de la Terre en présence d'une instabilité K–H générée par une résonance de ligne de champ autour de 10 rayons terrestres. Les résultats de l'analyse sont globalement en accord avec les observations et les modélisations numériques des sous-tempêtes. Partie de l'analyse, nous discutons l'importance de distinguer entre les propriétés de stabilité de la queue magnétique et le mécanisme de déclenchement de l'instabilité. Alors que ces deux éléments peuvent et sont probablement reliés, il est possible qu'ils impliquent différents types de mécanismes complémentaires.

[Traduit par la Rédaction]

Received 12 April 2006. Accepted 15 January 2007. Published on the NRC Research Press Web site at <http://cjp.nrc.ca/> on 14 February 2007.

P. Dobias^{1,2} and **J.C. Samson**. Department of Physics, University of Alberta, Edmonton, AB T6G 2J1, Canada. **J.A. Wanliss**. Embry-Riddle Aeronautical University, 600 S. Clyde Morris Blvd., Daytona Beach, FL 32114, USA.

¹Corresponding author (e-mail: peter.dobias@drdc-rddc.gc.ca).

²Present Address: DRDC CORA, Colonel By Dr., Ottawa, ON K1A 0A2, Canada.

1. Introduction

In the present work, we address the question of the nonlinear stability of the near-Earth plasma sheet before, during, and after a substorm onset. Dobias and Samson [1] outlined a possible sequence of events that take place during the substorm expansion phase. This sequence assumes an initiation of the expansion phase near Earth, once the near-Earth plasma sheet becomes unstable. They further suggested that the process responsible for the formation of a preexisting auroral arc (possibly field line resonance) is responsible for triggering the instability. While there are other opinions, we believe that the near-Earth initiation provides the simplest explanation for the observed sequence of events (see refs. 2 and 3 and refs. therein).

It has long been recognized that it is possible to understand the stability properties of dynamical systems without knowledge of a solution of the dynamical equations (see ref. 4 and refs. therein). One such approach utilizes energy-based methods of stability analysis. These methods have a long tradition in plasma physics going back to Bernstein et al. [5] and Arnold [6]. In this paper, we use a stability analysis approach suggested by Pfirsch and Sudan [7], improved further by Dobias and Samson [1].

This stability method can be summarized as follows. First, the plasma equilibrium to be studied is defined. In the second step the plasma perturbation is expressed in terms of a plasma displacement. All the other perturbed quantities can be expressed in terms of the displacement. The plasma displacement is used to calculate expansion terms in the potential energy density. Comparison of the terms yields the stability properties of the system [7]. If the second-order term is dominant, the system is well described by linear approximation. If the third-order term is dominant, the system is explosively unstable [7, 8]. The dominant fourth-order term means that the system is nonlinearly stable [8]. This method allows one to estimate the possible maximum growth of the instability before it is saturated by nonlinear effects [9].

To obtain an equilibrium related to realistic magnetospheric configurations, we use the Grad-Shafranov equation constrained by CANOPUS observations [10]. This ensures that our tested configurations are relevant for the substorm event we are analyzing, and includes implicitly many processes that influence the stability of the system (e.g., change in convection [11]). These are often neglected in the modeling of the magnetotail. We have to stress that we are not modeling a transition between equilibrium states, rather, we calculate each configuration as a separate equilibrium based on observations, thus avoiding limitations that would arise if we started with some specific equilibrium and allowed it to develop within some approximate model, for example, magnetohydrodynamics (MHD).

The above method was applied to analyze the nonlinear stability of the near-Earth plasma sheet during the 9 February 1995 substorm. We extend the previous work of Dobias et al. [12] by considering a possible development of the Kelvin–Helmholtz instabilities due to a strong velocity shear caused by field line resonances [13]. We analyze both changes in the stability properties of the plasma sheet due to the presence of a vortex, and a possible influence of the stability on the further development of this vortex. Our stability analysis is approximate, based on the ideal MHD, and it does not include influences of some other factors such as diffusion, Larmor radius effects, or the azimuthal pressure gradient. Furthermore, this method does not address the dynamics of the transition between stable and unstable configurations. Yet the results of this analysis are encouraging and point out some possible directions for future research.

As we deal with the stability of the near-Earth plasma sheet we suggest a possible explanation of how a slowly changing system can suddenly become explosively unstable. Hurricane et al. [14] argue that the problem with conventional approaches is that they do not provide sufficient explanation for the sudden occurrence of a nonlinearly unstable state and they suggest that a detonation type of phenomenon starting with a finite amplitude perturbation may be responsible for triggering the instability. We demonstrate that it is possible to have a time-dependent Hamiltonian system that is a subject to a very slow change that causes infinitesimally small modes to become explosively unstable on a very fast time scale (less than one period). For more detailed treatment of such systems in plasma physics see, for example, ref. 15 and references therein.

2. Stability of Hamiltonian systems and substorm triggers

To facilitate a deeper understanding of the stability of the Earth's magnetosphere during substorms, especially to stress a difference between the stability of the plasma sheet and the instability trigger itself, we begin with a discussion of the general stability properties of Hamiltonian systems [4, 16]. A detailed discussion of various types of stability and stability-analysis methods can be found in ref. 17. The following section is rather general, and is intended to frame the arguments for the stability analysis described in the subsequent sections.

A general dynamical system can be described in terms of generalized coordinates x and momentum p . These are functions of time and the dynamics can be pictured as a trajectory in phase space x - p . To obtain a temporal dependence of x and p one can define an energy function $H(x, p; t)$ (Hamiltonian). For a single particle system the Hamiltonian can be written as

$$H(x, p; t) = \frac{p^2}{2m} + V(x) \quad (1)$$

where m is the mass and $V(x)$ is the potential energy of the particle. The equations of motion for Hamiltonian systems can be written in the form

$$\frac{\partial x}{\partial t} = \frac{\partial H}{\partial p} \quad (2)$$

$$\frac{\partial p}{\partial t} = -\frac{\partial H}{\partial x} \quad (3)$$

At first, let us look at some special solutions of the Hamiltonian systems corresponding to a Hamiltonian

$$H(x, p) = \frac{p^2}{2m} - \alpha \frac{x^2}{2} + \beta \frac{x^3}{3!} + \gamma \frac{x^4}{4!} \quad (4)$$

where α , β , γ are some free parameters. In the simplest case only α is nonzero, and Hamiltonian (4) can be simplified to become

$$H = \frac{p^2}{2m} - \alpha \frac{x^2}{2} \quad (5)$$

Hamiltonian (5) corresponds to the equation of motion

$$m\ddot{x} = \alpha x \quad (6)$$

with either periodic solution $x = x_0 e^{\pm i\sqrt{\alpha}t}$ for $\alpha < 0$, or an exponentially growing and (or) decaying solution $x = x_0 e^{\pm\sqrt{\alpha}t}$ for $\alpha > 0$.

If only β is nonzero, Hamiltonian (4) becomes

$$H = \frac{p^2}{m2} + \beta \frac{x^3}{3!} \quad (7)$$

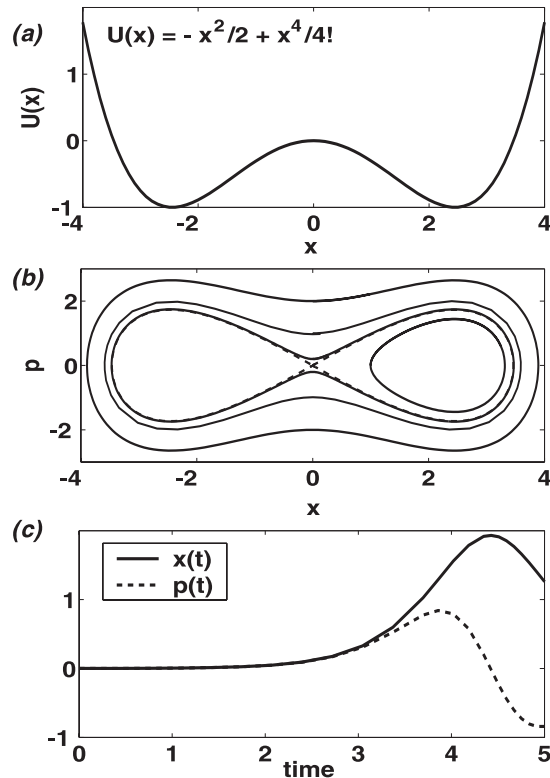
corresponding to the equation of motion

$$m\ddot{x} = -\beta \frac{x^2}{2} \quad (8)$$

Equation (8) allows for a singular solution

$$x = \frac{-6m}{\beta(t - t_C)^2} \quad (9)$$

Fig. 1. A Hamiltonian system that appears linearly unstable around $x = 0$, yet the system is stable. (a), the potential energy part of Hamiltonian $H = p^2/2m - x^2/2 + x^4/4$. (b), the orbits in phase space. There are two regions of a linear periodic motion, and one region of nonlinear oscillations. In between there is a linearly unstable region. (c), the time dependence of coordinate x (continuous line) and momentum p (broken line) for the motion passing through the linearly unstable region.

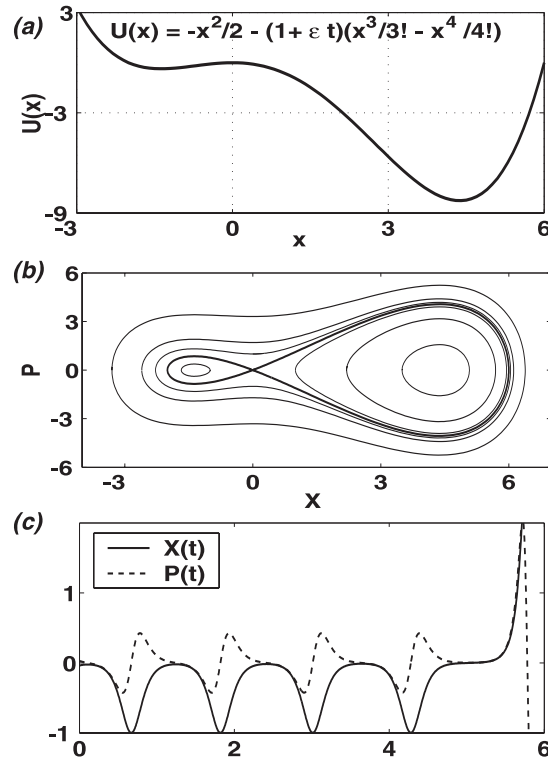


growing to infinity for a finite time t_C no matter what the sign of β is. This type of instability is called an *explosive instability* because of its extremely fast (progressively increasing) growth rate.

Another interesting situation arises when $\beta = 0$ and both α and γ are positive. It corresponds to a nonlinear potential well, with an exponentially growing solution while $|x| \ll 1$, but as the magnitude of x grows, the growth rate decreases, and eventually the system settles at nonlinear oscillations (Figs. 1b and 1c). Such a system would appear linearly unstable if subjected to a linear stability analysis assuming $|x| \ll 1$. Therefore, a linear stability analysis of the plasma sheet during the substorm growth phase might provide misleading results. Past studies, restricted to the linear approximation, suggest that the plasma sheet is always unstable [18]. Yet we demonstrate that the tail is actually (nonlinearly) stable. A closer look at the original Hamiltonian reveals that this linear instability would be saturated due to nonlinear effects.

Another interesting point we want to make is the importance of a distinction between destabilizing factors in the system and the immediate instability trigger. This distinction is crucial for proper understanding of the transition between stable and unstable configurations. Its importance is especially significant in a case of relaxation processes in which the energy is stored slowly in the system, and then released suddenly. In such cases the proper distinction between the trigger (dynamic mode that becomes unstable), and the stability properties of a system helps to address some of the concerns outlined in the literature, for example, that it is impossible to have a system that develops slowly from the linearly stable into a sudden onset of an explosive instability [14].

Fig. 2. Dynamical system with a time-dependent Hamiltonian $H = p^2/2m - x^2/2 - (1 + \epsilon t)(x^3/3! - x^4/4!)$. The originally stable mode becomes unstable as the Hamiltonian changes with time. (a), the potential energy at time $t = 0$; (b), the various types of orbits in phase space; and (c), the time dependence of coordinate x (continuous line) and momentum p (broken line) for the motion originating close to the separatrix between pseudolinear and the nonlinear oscillations. The system undergoes a period of explosive instability that is saturated due to the fourth-order term.



Consider a system described by the following time-dependent Hamiltonian

$$H(x, p, t) = \frac{p^2}{2m} - \alpha \frac{x^2}{2} - (1 + \epsilon t) \left(\beta \frac{x^3}{3!} - \gamma \frac{x^4}{4!} \right) \tag{10}$$

Figure 2a shows the potential energy part of Hamiltonian (10) at time $t = 0$. For a fixed time t , this system would yield a phase-space diagram like the one shown in Fig. 2b. Note that the system contains an x -line that separates the phase space into the three parts — two pseudo-linear and one nonlinear. The region around the x -point corresponds to the dominance of the third-order term in Hamiltonian (10). The difference in size between the two pseudo-linear areas defines the possible room for the growth of the displacement during a nonlinear (explosive) transition from a higher energy state to a lower energy state. It is apparent that as the Hamiltonian (10) varies slowly with time, the position of the x -line changes thus allowing the system originally confined in a smaller pseudo-linear area to transit to the nonlinear area. Depending on the parameter ϵ , this transition can be slow or fast. Fig. 2c shows an example of the system that developed slowly from a linear (stable) to an explosively unstable stage. Note that the position of the linear mode changes slightly, but the magnitude of the displacement does not change until the explosive stage. Also note that the exact shape of the displacement is not related to the stability properties of the system. These properties are given by parameters of the Hamiltonian.

This is very similar to observations of the substorm onset. It is possible to have a stable mode with a small amplitude in the system (for example, field-line resonances (FLRs) in the preexisting auroral arc),

and as the system develops from a stable to unstable configuration, the originally stable mode suddenly finds itself in an unstable area, bringing about global reconfiguration of the entire magnetotail.

3. Nonlinear stability of the near-Earth plasma sheet

3.1. Expansion of Lagrangian and stability analysis

There is a direct connection between the Hamiltonian and Lagrangian descriptions of dynamical systems. For fluid-like systems, these two descriptions correspond to the Eulerian and Lagrangian descriptions, respectively. The Lagrangian description is in terms of a generalized coordinate x and velocity \dot{x} and the Hamiltonian description is in terms of a coordinate and a momentum. The connection between Hamiltonian and Lagrangian descriptions is via Legendre transformation connecting coordinates (x, \dot{x}) with (x, p)

$$p = \frac{\partial H}{\partial \dot{x}} \quad (11)$$

and the Hamiltonian H with the Lagrangian L

$$H(x, p) = \dot{x}p - L(x, \dot{x}) \quad (12)$$

For dynamical systems with a potential energy independent of the velocity the Lagrangian can be expressed simply as

$$L = \frac{m}{2}\dot{x}^2 - V(x) \quad (13)$$

In the absence of convection, a Lagrangian in ideal MHD can be written in the above form. The connection between the Hamiltonian and Lagrangian descriptions ensures that the stability properties of the Hamiltonian systems extend to the Lagrangian description as well.

The stability properties of the system are decided according to the relative values of the energy-density terms in analogy with mechanical systems [7]. The entire stability analysis is built on the generic properties of the Hamiltonian and (or) Lagrangian systems, based on an analogy with mechanical systems. Although MHD systems are much more complicated, they can still be described in a similar functional form, substituting plasma displacement ξ for coordinates x . The Lagrangian in ideal MHD

$$L = \int \int \int dV \left(\frac{1}{2} \rho v^2 - \frac{1}{2\mu_0} B^2 \right) \quad (14)$$

can be expressed in terms of plasma displacement ξ defined as

$$\hat{x}(\mathbf{x}, t) = \mathbf{x} + \xi(\mathbf{x}, t) \quad (15)$$

Using conservation laws, $\xi(\mathbf{x}, t)$ is uniquely related to perturbed plasma quantities such as plasma pressure and magnetic field. In the absence of ambient convection (if the velocity is limited to the perturbation velocity $\mathbf{v} = \partial_t \xi$) the Lagrangian (14) can be expanded up to the fourth order in the plasma

displacement as

$$\begin{aligned}
 L(\xi) = & \int \int \int dV \left(\rho (\partial_i \xi)^2 - \left(\frac{p}{\gamma - 1} \left[1 + (1 - \gamma) \xi_a^a + \frac{1 - \gamma}{2} \left((1 - \gamma) \xi_a^a \xi_b^b + \xi_b^a \xi_a^b \right) \right. \right. \right. \\
 & + (1 - \gamma) \left(\xi_a^a \xi_b^b \xi_c^c - \gamma \xi_a^a \xi_b^b \xi_c^c + \frac{1}{6} \gamma (1 + \gamma) \xi_a^a \xi_b^b \xi_c^c \right) \\
 & + \frac{\gamma(\gamma - 1)}{2} \left(\xi_a^a \xi_b^b \xi_c^c \xi_d^d + 2 \xi_a^a \xi_b^b \xi_c^c \xi_d^d - (1 + \gamma) \xi_a^a \xi_b^b \xi_c^c \xi_d^d \right. \\
 & \left. \left. + \frac{1}{12} (\gamma + 1) (\gamma + 2) \xi_a^a \xi_b^b \xi_c^c \xi_d^d \right) \right] \\
 & + \frac{B^2}{2} \left[(1 - \xi_a^a) + \frac{1}{2} (\xi_a^a \xi_b^b + \xi_b^a \xi_a^b) + \xi_a^a \xi_b^b \xi_c^c + \xi_a^a \xi_b^b \xi_c^c \right. \\
 & - 2 \xi_a^a \xi_b^b \xi_c^c \xi_d^d + \xi_b^a \xi_a^b \xi_c^c \xi_d^d + \xi_a^a \xi_b^b \xi_c^c \xi_d^d + 2 \xi_b^a \xi_a^b \xi_c^c \xi_d^d \\
 & \left. + 2 \xi_a^a \xi_b^b \xi_c^c \xi_d^d - 2 \xi_b^a \xi_a^b \xi_c^c \xi_d^d + 2 \xi_a^a \xi_b^b \xi_c^c \xi_d^d \right] \\
 & + g_{ij} B^i B^j \left[\xi_l^j (1 - \xi_a^a + \xi_b^a \xi_a^b) + \xi_a^j \xi_l^a \xi_b^b - \xi_a^j \xi_a^a \xi_b^b \right. \\
 & \left. + 2 \xi_a^j \xi_b^a \xi_c^b \xi_c^c - \xi_l^j \xi_a^a \xi_b^b \xi_c^c - \xi_a^j \xi_b^a \xi_c^b \xi_c^c - \xi_a^j \xi_a^a \xi_b^b \xi_c^c \right] \\
 & \left. + g_{ij} B^i B^k \left[\xi_k^i \xi_l^j \left(1 - \frac{1}{2} \xi_a^a + \frac{1}{4} (3 \xi_b^a \xi_b^a - \xi_a^a \xi_b^b) \right) + \xi_k^i (\xi_a^j \xi_l^a \xi_b^b - \xi_a^j \xi_b^a \xi_l^b) \right] \right) \quad (16)
 \end{aligned}$$

In the above expressions, \mathbf{B} , p , ρ are the ambient magnetic field, the plasma pressure, and density. The expression X_j^i denotes $\partial X^i / \partial x^j$. Square brackets in indices $[i, j]$ denote antisymmetrization in indices i , and j .

If the second-order term in the expansion of the Lagrangian (16) is dominant, the corresponding equations of motion are linear, and the stability can be decided on the basis of the linearized analysis [18]. The linear analysis is not a point of interest for the present work since it was addressed in numerous previous works. If the third-order term is dominant, the system is explosively unstable, no matter what the sign of the energy density. By explosive instability, we understand a fast growing instability with the growth rate progressively increasing with the growth so that the system becomes singular in a finite time. The general form of such solution can be written as

$$\xi(x, t) = \frac{a}{(t - t_C)^\delta} \quad (17)$$

where a and δ are some real constants. The dominance of the fourth-order term may eventually slow down the growth, and may further lead to a nonlinear saturation of the instability. For systems with all the expansion terms nonzero, a range over which the displacement can increase between the dominance of the third-order term and the dominance of the fourth-order term suggests room for instability growth.

It is apparent that the most interesting situation for substorm dynamics is the one having the third-order term dominant over a large range of displacement. Such a system is likely to undergo a significant explosive instability causing a large-scale reconfiguration of the system. On the other hand, if the fourth-order term becomes dominant before the third-order term does, or after only a very short period of the dominance of the third-order term, the system is nonlinearly stable and no large-scale reconfiguration is likely to happen.

3.2. Grad-Shafranov equilibrium of magnetospheric plasmas

To perform the stability analysis, we use a Grad-Shafranov equilibrium. This means assuming the absence of an ambient flow and the equilibrium condition in the form

$$-\nabla\left(P + \frac{\mathbf{B}^2}{2\mu_0}\right) + \mathbf{B} \cdot \nabla\mathbf{B} = 0 \quad (18)$$

If the magnetic field is restricted to a plane (for example, azimuthally symmetric models), the expression (18) can be alternatively written in terms of two scalar potentials ψ and ϕ that define the magnetic field as [19]

$$\mathbf{B} = -\nabla\psi \times \nabla\phi \quad (19)$$

Then the equilibrium condition (18) becomes the Grad-Shafranov equation

$$\partial_{rr}\psi + \frac{\sin\theta}{r^2}\partial_\theta\frac{1}{\sin\theta}\partial_\theta\psi = 4\pi^2r^2\sin^2\theta\frac{\partial P}{\partial\psi} \quad (20)$$

which must be solved to obtain plasma equilibrium. The radius r , polar angle θ , and azimuthal angle ϕ are spherical coordinates. If we assume that the plasma pressure is a linear function of the magnetic flux ψ , we can use an approximate solution in the form of a sum of a dipolar solution and the solution valid for a magnetic field with a constant pressure gradient [10]

$$\psi(r, \theta) = 2\pi\frac{M\sin^2\theta}{r}\left[1 + \frac{1-\alpha}{2}\left(\frac{r}{R_X}\right)^3 + \frac{\alpha}{4}\left(\frac{r}{R_X}\right)^5\right] \quad (21)$$

This solution (21) is a reasonable approximation as far as the position of the x -line, but breaks down at larger distances. Its advantage is that it allows relatively simple correlation with experimental observations via adjustment of the two parameters α and R_X using the position of the proton isotropy boundary [20, 21], and the position of the red emissions obtained from CANOPUS ground-based observations [20]. This approach allows us to relate the theoretical equilibrium to a real magnetosphere in a very direct and yet workable way.

We use the distribution of auroral luminosity, from meridian-scanning photometer data, to gain information about the nature and location of various plasma boundaries in the magnetotail. As shown previously by Wanliss and co-workers [20, 22] meridian-scanning photometers are excellent tools for investigating precipitation of charged particles in the auroral ionosphere and can quite easily be used to constrain magnetospheric magnetic-field models. The precipitation of electrons and protons along magnetic-field lines into the auroral oval leaves ionospheric particles in excited states. Deexcitation of these particles is the main cause of auroral luminosity. The auroral luminosity patterns thus give one an indirect view of the motion of particles that are converging along magnetic-field lines from the magnetotail into the ionosphere.

The idea that we exploit in this paper relies on nonconservation of the first adiabatic invariant when magnetic field variations occur on the scale of a particle gyroradius. A measure of nonconservation is determined by the square root of the ratio of the magnetic-field-line radius of curvature to the particle gyroradius [23]. When this ratio is much less than one, as in the distant magnetosphere where the radius of curvature of the magnetotail field can be much smaller than the particle gyroradius, a particle can change its pitch angle as it is scattered through the current sheet. Much closer to the Earth the ratio can be larger than unity due to the large radius of curvature of the dipole magnetic-field lines. In between, there exists some transition between the taillike and dipolelike field configurations; Earthward of this transition location, particles in the current sheet are adiabatic, but they do not conserve their pitch angle tailward of this location. Theoretical effort by Zelenyi et al. [24] suggests that this transition occurs where the above ratio equals 3.

The work by Wanliss and co-workers [20, 22] searched for these transition locations in a model magnetotail and also in the more complicated Tsyganenko models. In addition to the need for a magnetic-field model, one can only find these locations if the energy of the precipitating particles is known. In our previous work, we used a range of energies with an average of about 20 keV for the precipitating protons that cause auroral emissions in the 486.1 nm band [25]. In the present work, the energies of the precipitating particles are determined directly from the equilibrium magnetotail model and are, therefore, no longer a free parameter.

Due to the nature of the model that utilizes the Grad-Shafranov equation, plasma pressure is one of the outputs. This is directly related to the temperature in the current sheet. We assumed a rather simple density profile that varied linearly from 1 cm^{-3} at $6 R_E$ to 0.1 cm^{-3} at the location of the last closed magnetic-field line in the distant magnetotail. Once this has been done, it is a simple matter to extract the temperature from the model and hence calculate the gyroradius and hence the transition location between adiabatic and nonadiabatic particle motion. The transition location in the magnetotail can then be mapped along a magnetic-field line to obtain the equivalent transition location in the ionosphere. The equatorward edge of the 486.1 nm emissions has been shown [25] to provide the ionospheric location to which the magnetotail transition region maps. Thus the model parameters can be varied to best match the ionospheric locations of the transition [22].

A new constraint is obtained from the model in that one of the model parameters is directly related to the location of the last closed magnetic-field line. This boundary can also be obtained from ground-based photometer data [26]. Blanchard et al. [26] demonstrated that the poleward border of 630.0 nm optical emissions is very close to the transition between open and closed field lines in the dusk–midnight sector. They fitted a step-function in latitude to the auroral emissions and compared the boundary of these photometer emissions with low-latitude Defense Meteorological Satellite Program (DMSP) particle measurements. The low-altitude trapping boundary was on average within $\pm 0.9^\circ$ of the poleward border of the 630.0 nm emissions. Blanchard et al. [27] assessed the validity of this method by examining an entirely different data set of these spacecraft and photometer comparisons and found that the identification of the poleward edge of the 630.0 nm emissions can be refined by adding a series of threshold values to the step-function criteria. They found that the average intensity of the red-line emissions in the polar cap was 60 Rayleighs (R) and in the auroral zone 160 R. Taking a threshold of 110 R, Blanchard et al. found that identifying the open-close boundary (OCB) as 0.7° equatorward of the 110 R transition, yields only a $\pm 1.2^\circ$ error in the majority of cases. In this present paper, we follow the same methodology to determine the ionospheric location of the last closed magnetic-field line.

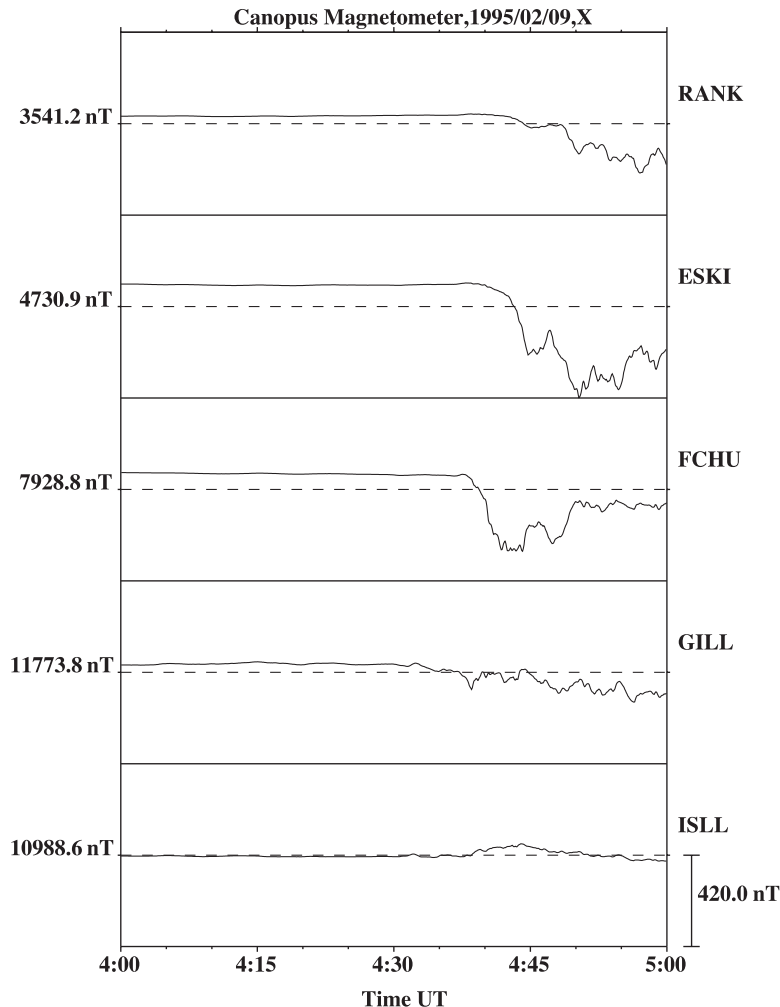
The magnetic-field model used in this paper has two free parameters that can be varied. Once an event has been selected for analysis, we calculate the equatorward edge of the 486.1 nm proton aurora, and the poleward edge of the 630.0 nm electron aurora as described above. Then the two free parameters in the magnetic-field model are varied via the Levenburg–Marquardt nonlinear optimization method to minimize the sum of the square of the error between the model boundaries and the boundaries obtained from the photometer data.

We decided to analyze the stability of the near-Earth plasma sheet during the 9 February 1995 event. For this event the substorm onset occurred approximately at 4:37 UT, with the first weak disturbances appearing between 4:30 and 4:35 UT (Fig. 3). For details of this substorm see ref. 28. We performed three stability tests. The first test was performed at 4:30 UT, just before any significant disturbances started occurring. The second test was performed for the 4:35 UT configuration, at the time just prior to onset. The last test we performed was after the onset at the beginning of the recovery phase at 4:40 UT. This was to look at the changes in the energy balance that the onset might have caused.

3.3. Plasma displacement for field line resonances and Kelvin–Helmholtz instability

Further, to perform the stability analysis, we needed to select a specific form of the plasma displacement ξ . Here, we extend the work in ref. 12 in which the authors performed analysis at several points

Fig. 3. CANOPUS magnetometer data for 9 February 1995. The substorm onset, marked by a sudden drop in magnetic field, starts around 4:37 UT.



during the late-growth phase assuming the plasma displacement corresponding to FLRs. However, Voronkov et al. [13] demonstrated that the presence of the 180° -phase shift in the velocity would lead to a development of the Kelvin–Helmholtz (KH) instability, that can be further coupled to ballooning modes. In the present paper, we study an impact of an FLR-generated KH instability on the overall stability of the near-Earth plasma sheet during the late-growth phase, and just prior to and after the substorm onset.

For the analysis we assume azimuthal symmetry. While not entirely consistent with the observations [11], since we are not attempting to resolve the transition between equilibrium states and we restrict our attention to a near-equatorial region, close to a single meridional plane [9], it is not an excessively restrictive assumption. We can observe stretching of the magnetotail (drop in the magnetic field, Fig. 4) and an increase in pressure gradient during the growth phase (Fig. 5). Note that there is a significant increase in plasma β between the 4:30 and 4:35 UT configurations.

We have chosen a location of the perturbation around $10R_E$, in the region where FLRs are most

Fig. 4. Magnetic field in the equatorial plane for 4:30, 4:35, and 4:40 UT configurations. The dotted line shows the dipolar field for reference. The field lines are being stretched, this is marked by a drop in magnitude in the near-Earth region.

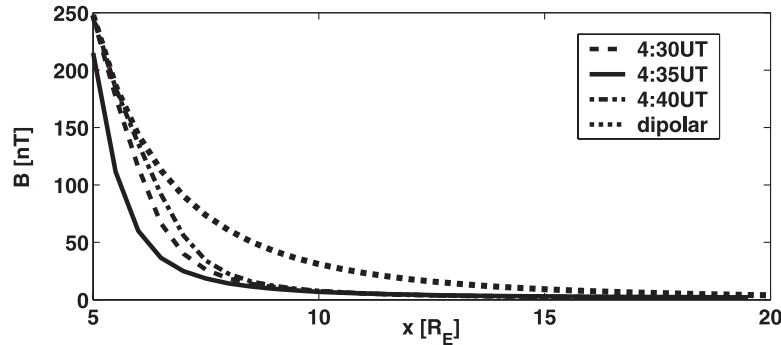
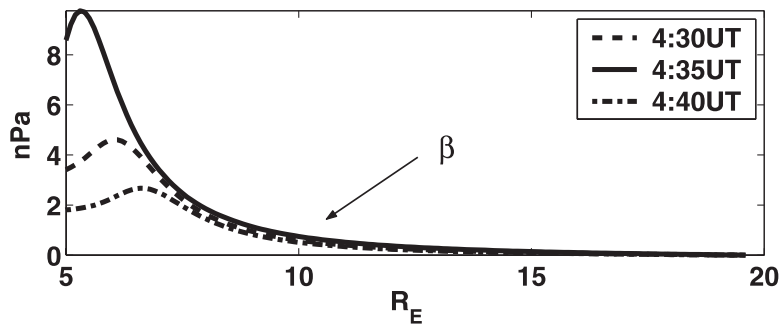


Fig. 5. Plasma pressure in the equatorial plane for 4:30, 4:35, and 4:40 UT configurations. The pressure gradient increases and the region of maximum pressure is moving Earthward. The value of plasma β at $10R_E$ is 14 for the 4:30 UT, later it increases to 40 for 4:35 UT, and then drops to 10 for the 4:40 UT configuration.



likely to occur [29]. Plasma displacement due to FLRs can be written in components as

$$\xi_r = \xi_{r0} \ln((x - x_r) + i\epsilon) \tag{22}$$

for the radial, and

$$\xi_\phi = \frac{\xi_{\phi 0}}{x - x_r - i\epsilon} \tag{23}$$

for the azimuthal component of the plasma displacement in the equatorial plane. In expressions (22) and (23), $x_r (= 10R_E)$ is the position of the resonance and ϵ is a small parameter that prevents a singularity and is related to the energy losses in the system.

A velocity shear in fluid and plasmas always leads to development of KH instability [30]. Thus, the 180° -phase shift in the resonance will cause development of a KH instability in the region [13]. This is also in accordance with observations and numerical simulations [31, 32].

The development of a KH instability along the azimuthal position of the resonance has a two fold effect on the dynamics of the displacement. First, it increases the gradients of the plasma displacement due to a development of vortex structures. Second, another effect of the vortex wrapping is a redistribution of the kinetic energy, and subsequent suppression of the displacement growth. If the KH instability is coupled to a ballooning type instability, the growth can continue as the shear flow-ballooning instability [13].

To model a development of the KH instability, we use a fluid approximation. This is justified by the fact that our analysis is restricted to the equatorial plane where the magnetic field is perpendicular to the velocity field, and thus there is no wrapping of magnetic-field lines. Initial stages of the KH instability can be easily modeled analytically. We can assume a surface of discontinuity along the y direction, with the velocity equal $\pm U$ along the surface. Then the temporal development can be described by ref. 33

$$x(y, t) = \alpha e^{\gamma t} \cos ky \quad (24)$$

However, the expression (24) exhibits unbound growth and lacks any wrapping of the surface of discontinuity that characterizes a realistic KH instability [34, 35]. To model the KH instability into its nonlinear stage we can use a semi-analytical approach first presented by Rosenhead [36]. It is based on approximating the surface of discontinuity by a series of elementary vortices. This method is widely used nowadays in computational fluid dynamics (see, for example, ref. 37). It is sufficient to introduce this method once the displacement is too great for a linear approximation. Thus, we can start with a displacement described by (24), and let it dynamically develop into a vortex.

The x and y components of velocity (u_a, v_a) of the a th vortex can then be calculated as [36]

$$u_a = -\frac{U}{n} \sum_{i \neq a} \frac{\sin \frac{2\pi}{\lambda}(y_a - y_i)}{\cosh \frac{2\pi}{\lambda}(x_a - x_i) - \cos \frac{2\pi}{\lambda}(y_a - y_i)} \quad (25)$$

$$v_a = \frac{U}{n} \sum_{i \neq a} \frac{\sinh \frac{2\pi}{\lambda}(x_a - x_i)}{\cosh \frac{2\pi}{\lambda}(x_a - x_i) - \cos \frac{2\pi}{\lambda}(y_a - y_i)} \quad (26)$$

In the expressions (25) and (26) U , is the velocity of the flow along the surface of discontinuity, n is the number of elementary vortices, and (x_i, y_i) are the coordinates of the remaining elementary vortices. Once we know velocities of the elementary vortices, we can calculate the time development of the surface of discontinuity by solving a set of ordinary differential equations

$$\dot{x}_a = u_a(x, y) \quad (27)$$

$$\dot{y}_a = v_a(x, y) \quad (28)$$

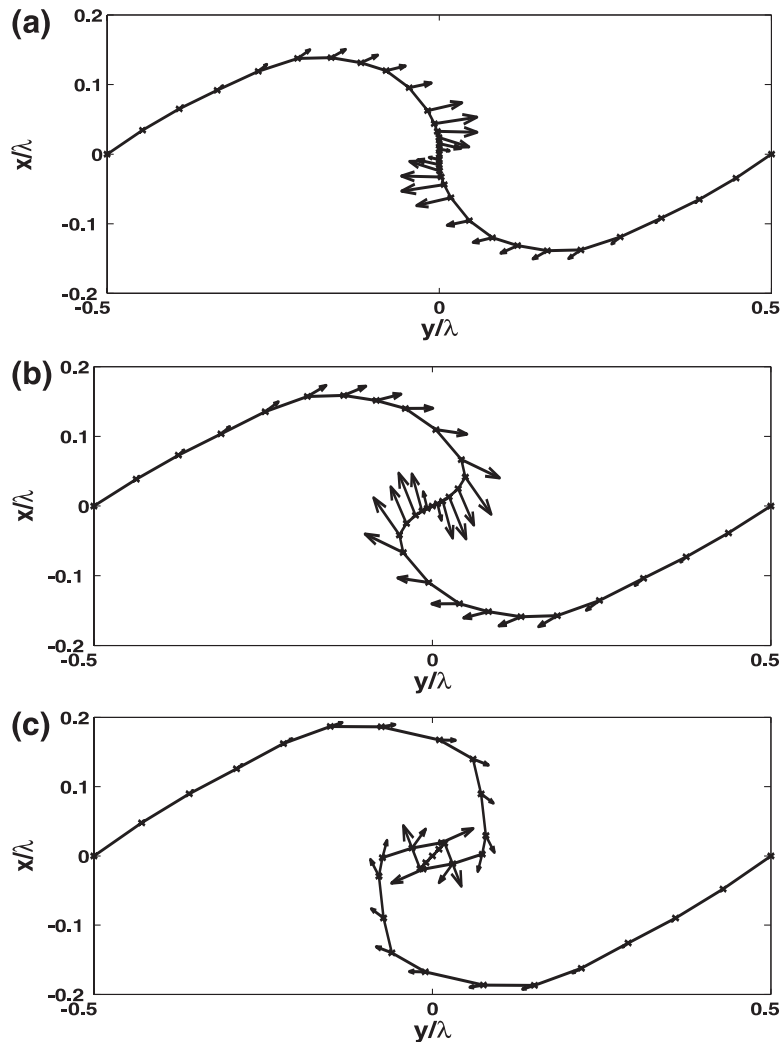
Equations (27) and (28) describe a change in the position of the vortex sheet with time due to the presence of finite velocity components at the surface of the discontinuity. Figure 6 shows the development of the surface of discontinuity including the direction of velocity vectors.

Once we are able to calculate temporal development of the KH vortex, we are ready to model coupling between the FLRs and the KH instability. For simplicity, we can assume that the resonance introduces a velocity shear $\pm |u_{\phi\text{FLR}}|$ along the azimuthal direction. Since we are dealing with the dynamics close to the midnight plane, we can approximate the plasma sheet by a box model, with positive x in the tailward direction and y in the azimuthal direction. Then the surface of discontinuity is in the y -direction at the position of resonance, x_r . Since the resonance introduces a small radial perturbation (22) in the x -direction, the KH instability develops. We can assume that during the linear stage this surface is displaced according to expression (24) introducing a sinusoidal displacement along the y -direction. Then we can use equations (27) and (28) combined with the expressions (25) and (26) to obtain profiles of various stages of the KH instability. Then we can use these profiles to calculate the energy densities for the stability analysis.

3.4. Results of stability analysis

We performed the stability analysis in several stages. At first we assumed that a FLR was formed at $10R_E$. We tested the stability of the system using the potential energy density from Lagrangian (16). Allowing the magnitude of the resonance ranging between $0.5R_E$ and $2R_E$. The choice was made

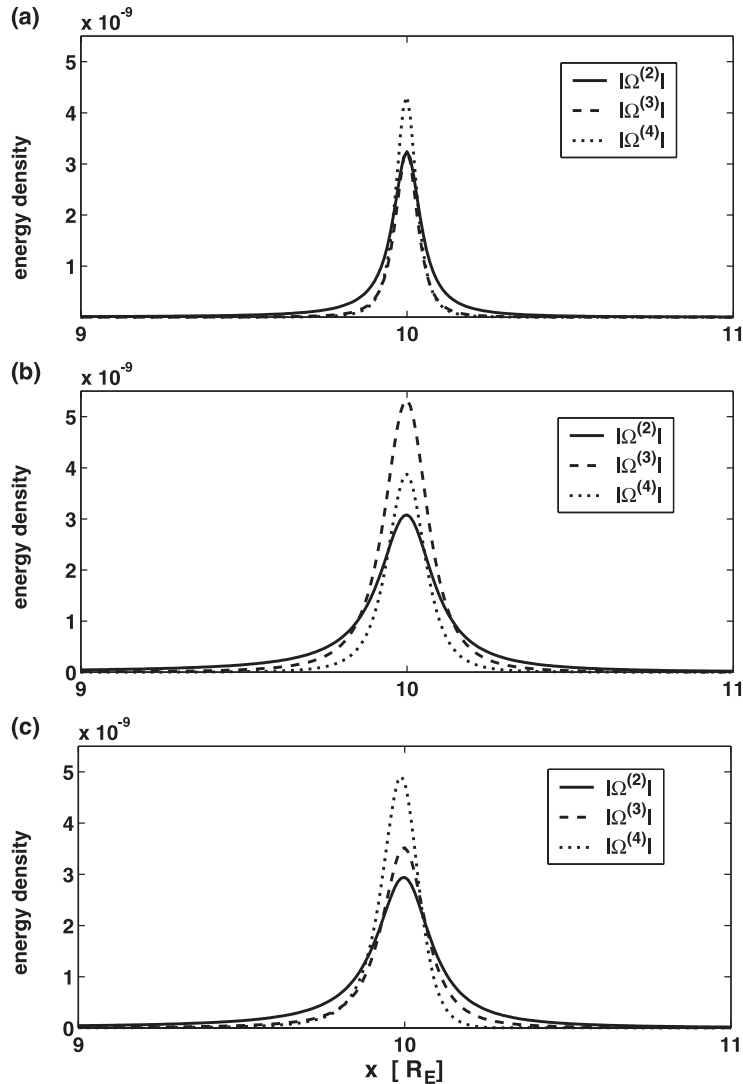
Fig. 6. Development of Kelvin–Helmholtz instability in equatorial plane. The distance in the x and y directions is normalized in terms of wavelength λ of the instability. The wrapping of the surface of discontinuity is clearly visible at the later stages of the development. The magnitude of the displacement is approximately 0.2λ . The ambient velocity is scaled to be ± 1 .



so that the initial magnitude would lie in the linear range (dominant second-order term) for all the configurations.

For the 4:30 UT configurations the dominance of the second-order term was followed directly by the dominance of the fourth-order term. The third-order term was never the most important term. This meant that there was no free energy available for the explosive instability, and any possible linear instability [18] would be quickly saturated by nonlinear effects before it could cause any observable reconfiguration of the magnetotail. Thus, the near-Earth plasma sheet was stable with respect to a FLR type of displacement for this configuration. For the 4:35 UT configuration, the situation was much different. The third-order term in energy began dominant for displacement magnitudes surpassing $0.75R_E$. It maintained its dominance almost until $2R_E$ before the fourth-order term became dominant. This allowed a global

Fig. 7. Potential-energy density for the FLR type of the displacement in the equatorial plane. The magnitude of the displacement is $1R_E$. (a) and (c), corresponding to 4:30 UT and 4:40 UT configurations, respectively, exhibit stable behavior, with the fourth-order term dominant, while (b), corresponding to the 4:35 UT configuration, contains a dominant third-order term that means that this configuration is explosively unstable.



reconfiguration of the system. However, the 4:40 UT configuration behaves in a fashion similar to the 4:30 UT configuration. The dominance of the second-order term was followed directly by the dominance of the fourth-order term. It showed that by this time, the excess energy was released and the system was back in the lower energy state where it had been before the onset. Figure 7 shows the energy densities for the magnitude of the displacement of $1R_E$. The third-order term is clearly dominating in the plot 7b corresponding to 4:35 UT configuration. For all other configurations the fourth-order term is dominant.

Further, we assumed that the velocity shear due to FLR led to a development of a KH instability. We started with the magnitude of the resonance at $0.75R_E$. As was discussed earlier, the magnitude

of the displacement specified the magnitude of the velocity shear. Then we assumed that there was a perturbation in the radial direction that initiated development of the vortex (Fig. 6). For the stability analysis we chose the three stages of the vortex development shown in Fig. 6. Then we repeated tests with the initial magnitude of the FLR at $1R_E$. The presence of the KH instability led to broadening of the disturbed region, propagating the perturbation further away from the site of the resonance. Again, the initial magnitude of resonance was $0.75R_E$, ensuring that the initial energy density was in the linear regime. Just as in the case of a FLR type of displacement, for the 4:30 UT configurations the dominance of the second-order term was followed directly by the dominance of the fourth-order term as the development of the vortex progresses. It meant that any instability growth would be saturated due to nonlinear effects. For the initial magnitude of the displacement at $1R_E$ we obtained similar results, with the difference that the fourth-order term was dominant from the onset of the KH instability.

For the 4:35 UT configuration, the start, with the initial magnitude of the FLRs at $0.75R_E$, ensured that the initial energy density was in the linear regime (dominant second-order term). However, even for the initial stages of the KH instability, the third-order term was much more important than for the pure resonance-type displacement. Further, development of the vortex led to a strong dominance of the third-order term. This meant that the presence of the vortex further destabilized the near-Earth plasma sheet. For the initial magnitude of the resonance of $1R_E$, even the initial stages of the vortex development led to a dominant third-order term in the energy density. We obtained the strongest dominance of the third-order term for stage (c) (Fig. 6) of the vortex development. Further, wrapping of the vortex led to dominance of the fourth-order term, which meant that it provided a stabilizing effect on the system.

The results of the analysis of the 4:40 UT configuration were similar to the results at late growth phase. The initially dominant second-order term for early stages of the vortex development were followed by the dominance of the fourth-order term. This confirmed that at this stage the excess energy was already released and the system was back in the lower energy state.

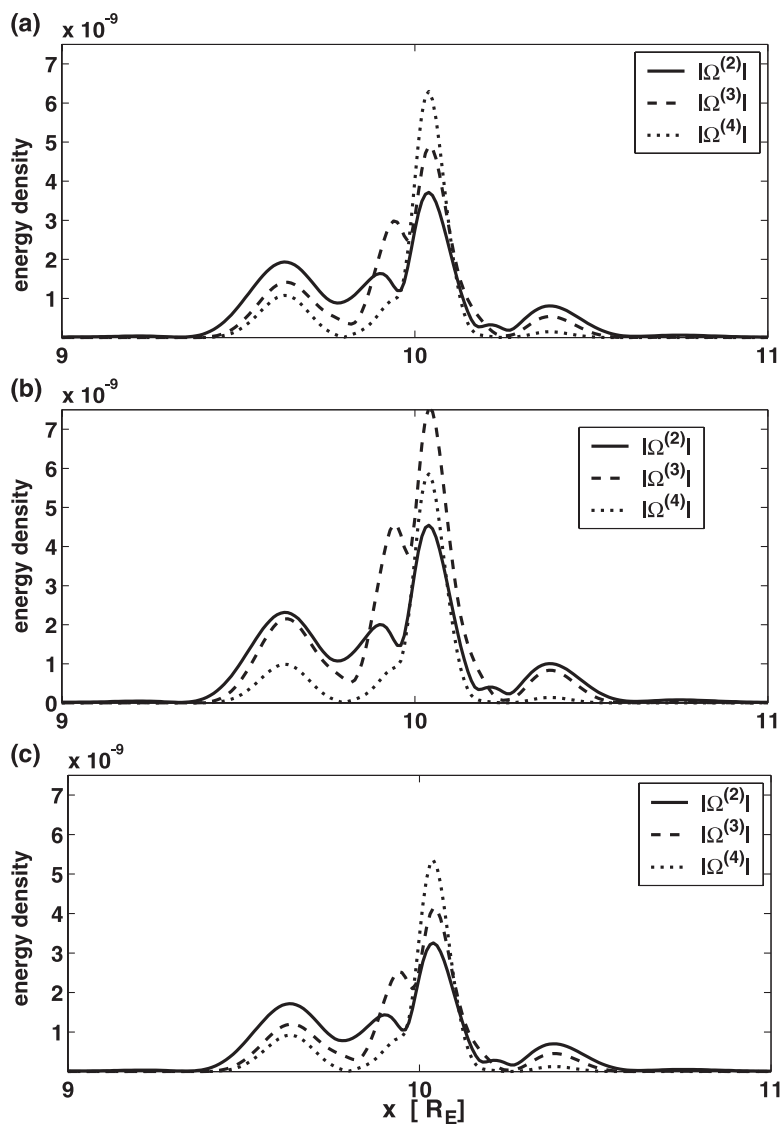
Figure 8 shows the results for the magnitude of the resonance set at $0.75R_E$ for the most unstable stage of the vortex (Fig. 6c) for all four configurations. For the 4:35 UT configuration, the third-order term was dominant while for all the other configurations the fourth-order term is dominant. Thus, only the 4:35 UT configuration, just minutes prior the onset, is explosively unstable, while during the growth phase and the recovery phase the near-Earth plasma sheet was nonlinearly stable.

Since a KH instability does not extract potential energy, only redistributes the kinetic energy, a presence of the KH instability alone cannot explain the energy reconfiguration in the near-Earth plasma sheet. Note that in Fig. 6, the presence of the vortex wrapping led to a saturation of the magnitude of the displacement. Voronkov et al. [13] propose that a coupling between the KH and the ballooning modes could lead to a growth of the vortex and thus to extraction of the energy from the region.

To test the effect of this scenario on the change in the stability properties, we assumed an increase in the size of the vortex, and calculated the energy density for such configurations. Figure 9 shows the energy density terms for a vortex that grows to twice its original size. Figures 9a and 9b correspond to vortex sizes of $1R_E$ and $2R_E$. As the vortex grew, the fourth-order term in energy became dominant, suggesting nonlinear saturation of the instability. This result agreed with the scenario of extraction of energy by a KH-ballooning coupling and was consistent with the computational model of the shear-flow-ballooning instabilities and observations of auroral arcs [13, 38].

To summarize, the development of the KH instability from the velocity shear due to field-line resonance provided similar stability properties for various stages of the 9 February 1995 substorm as did the field-line resonance alone. This suggests that these general stability results are not dependent on a precise plasma displacement, and that any realistic displacement would potentially lead to the explosively unstable near-Earth plasma sheet minutes prior to the onset. However, to fully address the question of the saturation of the instability and the plasma-sheet dynamics at later stages of the substorm expansion phase, a mode conversion and various types of hybrid instabilities need to be considered. It is likely that at later stages hybrid ballooning-tearing modes might develop, thus affecting the character

Fig. 8. Potential-energy density in the presence of a pre-existing Kelvin–Helmholtz instability in the equatorial plane. The magnitude of the displacement due to initial FLR is $0.75R_E$. The figure corresponds to part (b) of the Fig. 6, which is the most unstable type of displacement. The cross section is taken through the region of maximum velocity gradient. Parts (a) and (c), corresponding to 4:30 UT and 4:40 UT configurations, respectively, show stable behavior, with the fourth-order term dominant, while part (b), corresponding to 4:35 UT, contains a dominant third-order term that means that this configuration is explosively unstable. The perturbed region is wider than that of resonance.

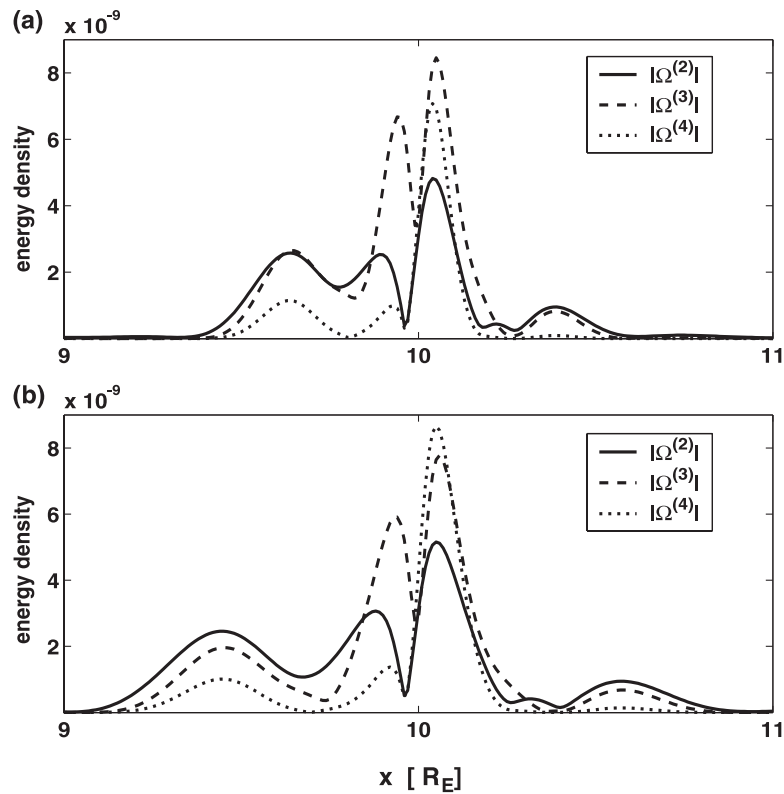


and topology of the magnetosphere. To investigate that is beyond the scope of this paper.

4. Conclusions

We present an analysis of the stability of the near-Earth plasma sheet in the presence of field-line resonances (FLR) and the FLR-induced Kelvin–Helmholtz (KH) instability. Our results suggest that

Fig. 9. Potential energy density for the 4:35 UT configuration for the Kelvin–Helmholtz type of the displacement. The initial magnitude of the FLR is $1.00R_E$. We allowed growth of the size of the vortex as if the Kelvin–Helmholtz instability was coupled to a ballooning type mode. (a) corresponds to the same width of the vortex approximately $1R_E$, while (b) corresponds to the width of the vortex $2R_E$. The growth of the vortex lead to the dominance of the fourth-order term in energy, thus to saturation of the instability.



during the stable state of a substorm (late growth phase) the presence of a KH vortex would not influence the stability of the system. Since there is not enough free energy available, such a vortex would not grow. In the case of the unstable configuration during the onset, the presence of a KH instability causes a faster initiation of the explosive instability because of enhanced gradients of the plasma displacement.

However, we need to note that the KH instability could be initiated by any velocity shear, and thus it does not have to be tied to the FLRs. On the other hand, if there is resonance present, the KH instability will appear. The KH instability alone cannot extract potential energy from the system. It only transforms different forms of kinetic energy. Therefore, we investigated what would happen if the vortex grew due to a possible coupling of the KH instability with ballooning modes. It appears that the growth of the vortex would eventually lead to the extraction of the energy, and the saturation of the instability. We can conclude that for the event studied, the transition between stable and unstable configurations corresponded to the time of onset no matter what the displacement was. It was also demonstrated that at the early recovery stage the plasma sheet becomes stable again.

In our analysis, we did not explicitly consider various influences such as the coupling with the solar wind or dynamical internal changes in the magnetosphere. However, these factors are included implicitly, in constraining the theoretical equilibrium, by the CANOPUS observations. Furthermore, our discussion of the stability of the Hamiltonian systems pointed out the importance of the distinction

between the substorm trigger and factors influencing the stability of the system. A proper distinction between these two allows for an explanation of seeming problems with the slow energy storage followed by a sudden onset of an explosive instability. Also, we believe that a proper distinction between the two aspects of substorm dynamics allows for a better explanation of other features observed such as the pre-existence of stable auroral arcs. The factors influencing stability can be both internal and external. The external factor can be, for example, changes in convection due to the reversal in the interplanetary magnetic field [11]. Internal factors can include dynamical changes in the system, changes in the pressure balance, etc. Most likely, both internal and external influences should be included in the consideration. One has to remember that the magnetosphere is not a closed system, but that it interacts with the solar wind and with the ionosphere.

One of the well-established facts about substorms is that the onset has to occur within the pre-existing auroral arc. Such arc is probably related to the trigger directly responsible for a substorm onset once a plasma sheet reaches an explosively unstable state. Reference 39 shows that some auroral arcs are formed by FLRs; but the work is not conclusive and the question of the auroral arcs remains open [40]. The fast 180° -phase shift in the resonance might be an important factor in faster development of the instability once the system reaches unstable state. Therefore, it has been suggested that FLRs are responsible for triggering the instability [10]. However, the question of triggers still remains open and there is yet no general consensus on the topic of a substorm trigger.

We demonstrated that it is possible to connect the substorm onset with the explosive ballooning-type instability triggered by a resonant process at about $10R_E$. More work addressing a transition from the stable to unstable stage, and especially the influence of various additional internal and external factors needs to be assessed. Also, a mode conversion involving development of tearing modes leading to a reconnection must be addressed to adequately describe the later stages of the expansion phase.

Acknowledgments

This research was funded by the Natural Sciences and Engineering Research Council of Canada (NSERC). Work by JW was partially supported through NSF grant ATM-0449403. CANOPUS is an array funded by the Canadian Space Agency (CSA).

References

1. P. Dobias and J.C. Samson. *Can. J. Phys.* **82**, 593 (2004).
2. S.I. Akasofu. *Planet. Space Sci.* **12**, 273 (1964).
3. L.R. Lyons, I.O. Voronkov, E.F. Donovan, and E. Zesta. *J. Geoph. Res.* **107**, 1390 (2002).
4. J.E. Marsden and T.S. Ratiu. *Introduction to mechanics and symmetry*. Springer-Verlag, New York. 1999.
5. I.B. Bernstein, E.A. Frieman, M.D. Kruskal, and R.M. Kulsrud. *Proc. R. Soc. London A*, **17**, 244 (1958).
6. V.I. Arnold. *Am. Math. Soc. Transl.* **79**, 267 (1969).
7. D. Pfirsch and R.N. Sudan. *Phys. Fluids*, **7**, 2052 (1993).
8. B.H. Fong, S.C. Cowley, and O.A. Hurricane. *Phys. Rev. Lett.* **82**, 4651 (1999).
9. P. Dobias, I.O. Voronkov, and J.C. Samson. *Phys. Plasmas*, **11**, 2046 (2004a).
10. J.C. Samson and P. Dobias. *In Multiscale Coupling of Sun–Earth Processes. Edited by A.T.Y. Lui, Y. Kamide, and G. Consolini*. Elsevier, Amsterdam. 2004. p. 235.
11. L.R. Lyons, C.-P. Wang, T. Nagai, T. Mukai, Y. Saito, and J.C. Samson. *J. Geoph. Res.* **108**, doi:10.1029/2003JA010177 (2003).
12. P. Dobias, J.A. Wanliss, I.O. Voronkov, and J.C. Samson. *In Proceedings of the 7th International Conference on Substorms. 21–27 March 2004, Levi, Finland. Edited by N. Ganushkina and T. Pulkkinen*. Finnish Meteorological Institute, Helsinki. 2004. p. 152.
13. I. Voronkov, R. Rankin, P. Frytz, V.T. Tikhonchuk, and J.C. Samson. *J. Geoph. Res.* **102**, 9639 (1997).
14. O.A. Hurricane, B.H. Fong, and S.C. Cowley. *Phys. Plasmas*. **4**(10), 3565 (1997).
15. J.D. Crawford. Ph.D. thesis, University of California, Berkeley 1983.
16. L.D. Landau and E.M. Lifshitz. *Mechanics*. 3rd ed. Pergamon Press. 1976.

17. D.D. Holm, J.E. Marsden, T.S. Ratiu, and A. Weinstein. *Phys. Rep.* **123**, 1 (1985).
18. W.W. Liu. *J. Geophys. Res.* **102**, 4927 (1997).
19. L.D. Landau and E.M. Lifshitz. *Elektrodinamika sploshnykh sred.* Nauka, Moscow. 1992.
20. J.A. Wanliss, J.C. Samson, and E. Friedrich. *J. Geophys. Res.* **105**, 27 673 (2000).
21. E.F. Donovan, B.J. Jackel, I. Voronkov, T. Sotirelis, F. Creutzberg, and N.A. Nicholson. *J. Geophys. Res.* **108**, 1115 (2003).
22. J.A. Wanliss, R. Rankin, J.C. Samson, and V.T. Tikhonchuk. *J. Geophys. Res.* **107**, 10.1029 (2002).
23. J. Büchner and L.M. Zelenyi. *J. Geophys. Res.* **92**, 13 456 (1987).
24. L. Zelenyi, A. Galeev, and C.F. Kennel. *J. Geophys. Res.* **95**, 3871 (1990).
25. J.C. Samson. *In Proceedings of the International Conference on Substorms 2.* 7–11 March 1994, Fairbanks, Alaska. *Edited by* J.R. Kan, J.D. Craven, and S.I. Akasofu. University of Alaska, Fairbanks. 1994. p. 189.
26. G.T. Blanchard, L.R. Lyons, J.C. Samson, and F.J. Rich. *J. Geophys. Res.* **100**, 7855 (1995).
27. G.T. Blanchard, L.R. Lyons, and J.C. Samson. *J. Geophys. Res.* **102**, 9697 (1997).
28. E. Friedrich, J.C. Samson, I. Voronkov, and G. Rostoker. *J. Geophys. Res.* **106**, 13145 (2001).
29. J.C. Samson, L.L. Cogger, and Q. Pao. *J. Geophys. Res.* **101**, 17373 (1996).
30. S. Chandrasekhar. *Hydrodynamic and hydromagnetic stability.* Oxford Press, Oxford. 1961.
31. R. Rankin, P. Fritz, J.C. Samson, and V.T. Tikhonchuk. *Phys. Plasmas*, **4**, 829 (1997).
32. J.A. Wanliss and R. Rankin. *Earth Planets Space*, **54**, 927 (2002).
33. H.H. Lamb. *Hydrodynamics.* Cambridge University Press, Cambridge. 1932.
34. J. Jeffreys. *Proc. R. Soc. London A*, **107**, 190 (1925).
35. H. Jeffreys. *Proc. R. Soc. London A*, **128**, 383 (1930).
36. L. Rosenhead. *Proc. R. Soc. London A*, **134**, 170 (1931).
37. J.D. Anderson. *Fundamentals of aerodynamics.* McGraw–Hill. 2001.
38. I. Voronkov, E.F. Donovan, B.J. Jackel, and J.C. Samson. *J. Geophys. Res. A*, **105**(8), 18 505 (2000).
39. J.C. Samson, R. Rankin, and V.T. Tikhonchuk. *Annales Geophys.* **21**, 933 (2003).
40. I.O. Voronkov, E.F. Donovan, P. Dobias, V.I. Prosolin, M. Jankowska, and J.C. Samson. *In Proceeding of the 7th International Conference on Substorms.* 2004. 21–27 March 2004, Levi, Finland. *Edited by* N. Ganushkina and T. Pulkkinen. Finnish Meteorological Institute, Helsinki. 2004. p. 140.